

Large aperture x-ray refractive lens from lithium.

N. R. Pereira^a, E. M. Dufresne^{b,c}, D. A. Arms^c and R. Clarke^b

^a Ecopulse, Inc., PO Box 528, Springfield, VA 22150 USA;

^b Department of Physics and MHATT-CAT, University of Michigan, Ann Arbor, MI 48109-1120;

^c Advanced Photon Source and MHATT-CAT, Argonne, IL 60439;

ABSTRACT

Lithium promises to give refractive x-ray optics the highest possible transmission, aperture and intensity gain. Room-temperature embossing of lithium with parabolic dies from polypropylene produces lenses that focus well but are not yet good enough for imaging. X-ray measurements suggest two causes of problems, one of which one can be solved easily.

Keywords: x-ray, refraction, lens, lithium

1. INTRODUCTION.

Manipulating highly collimated x-ray beams from synchrotrons with refractive optics was suggested more than a decade ago,¹ and demonstrated to be practical a few years later.² The secret is to deflect the x-rays many times, with a series of refracting structures that approximates a gradient index lens for x-rays.³ In the last 10 years various groups have made increasingly better refractive x-ray optics. In particular, the x-ray optics group at Aachen University has built excellent cylindrically symmetric parabolic lenses⁴ that can be used not only for collimation or focusing, but also for imaging and microscopy.⁵⁻⁷

Cederstrom's multiprism^{8,9} approximates a one-dimensional parabolic profile on the fly, with an array of prisms placed under a small angle with respect to the x-ray beam. Multiprisms are easier to make than parabolas, and its focal length is variable because it depends on the multiprism's orientation.

X-ray refractive lenses made with silicon, aluminum and plastics are limited by attenuation in the lens material.¹⁰ Of the conventional materials beryllium offers the lowest attenuation, and good beryllium lenses are now available as one-dimensional multiprisms and two-dimensional parabolas. Micromachining techniques make it possible to construct lenses in silicon and plastics, with intricate features that allow shorter focal length without excessive absorption.

X-ray lenses produced with conventional techniques should have larger apertures and better x-ray transmission when made from lithium,¹¹⁻¹⁴ hence make superior collimators. However, x-ray lenses made from lithium have not yet performed at their theoretical potential. In particular, their intensity gain is an order of magnitude lower than expected because the lens gives a larger spot size than should be possible.

There seem to be two principal reasons for the discrepancy. One is deviations from the proper lens figure that results in macroscopic aberrations, the other is a widening related to the lens's local properties. The large-scale aberrations are consistent with random alignment and fabrication errors of the individual lenslets. Widening of the image is consistent with small-angle x-ray scattering that is most likely caused by surface roughness of the die.

The lens in this paper is a Compound Refractive Lens (CRL) made up from 76 individual lenslets. Figure 1 shows the lens package. It is a vacuum nipple with standard 2 3/4 inch (70 mm) UHV conflat flanges filled with dry helium. X-rays enter and exit the lens through 0.126 μm thick and 10 mm diameter beryllium windows behind the protective plastic covers. The nipple's glass center makes it possible to see the lithium foil that is wrapped around the lens stack. The foil acts as a getter: it should corrode before the lithium in the lens does,

Corresponding author: pereira.at.ecopulse.com



Figure 1. Packaging of the lithium lens inside a hermetic enclosure.

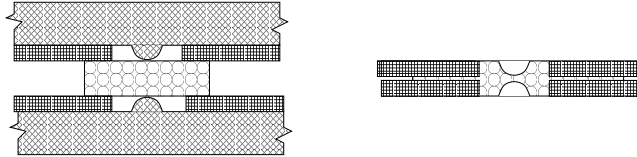


Figure 2. Embossing lithium lenslets: before (left) and after (right).

hence a visibly clean lithium foil implies that the invisible lithium inside the lens is clean too. The lenslets are aligned on three steel rods, one of which presses the lenslets against the others from outside the foil.

Figure 2 illustrates how the lenslets are made. A 1 mm thick lithium disk with $\simeq 5$ mm diameter (lightly hatched) is placed between two steel fender washers (dark hatching). The washers are 20 mm in diameter and have a 2 mm diameter hole in the center that accommodates the lithium. parabolic tips on otherwise flat plastic dies are centered on the washers, and pressing the dies together squeezes the lithium from between the washers onto the parabolas.

The right side of Figure 2 sketches a finished lenslet. Each has two concave parabolas. The parabola's diameter d at the top is $d = 1$ mm, and its height h is just under 0.5 mm. Parabolas are better than spheres as emphasized by the Aachen group: parabolic lenses don't have spherical aberrations, the parabola's aperture $d = 2\sqrt{2Rh}$ is not solely dependent on the focal length $f \propto 1/R$, and the force from a parabolic die pushed into a flat plate always has a component perpendicular to the die's surface. In the approach here the lithium flows around the die, so that the latter argument applies only indirectly: after the lithium has filled the volume around the parabolic die, the die can be pulled out cleanly because axial motion implies radial separation. Lithium always sticks a little bit, and it is wise to limit the maximum angle at the parabola's top, to $\pi/3$. The parabola's radius of curvature then becomes $R \simeq 0.263$ mm.

The parabola's tops are separated by layer of lithium in between the parabolas that is about $d \simeq 100 \mu\text{m}$ thick. In between the washers the lithium layer is thinner, as determined from the pressure used in the embossing, the deformation of the plastic die and of the washers, and the flow of the lithium including its adhesion to the washer surface. The CRL package of Figure 1 has about 100 mm space in between the flanges, just enough room for 76 lenslets and the spring that keeps them under axial pressure.

Embossing is done at room temperature. Lithium flows easily at room temperature, although there is some work hardening.¹⁵ Lithium has a body-centered cubic (bcc) crystalline structure, and such metals usually anneal at around $2/3 T_m$. For lithium $T_m = 453$ K and $2/3 T_m \simeq 29^\circ\text{C}$, hence room-temperature extrusion and embossing of lithium should leave the lithium fully annealed and with uniform density. Lithium's metallurgy is known through a series of papers^{16, 17} that emphasize lithium's unique status as a model metal but do not treat lithium as an x-ray optical material. Their work, and x-ray diffraction on a freshly extruded 3 mm thick strip, suggests that room-temperature lithium crystals are about 1 mm, comparable to a lithium lenslet.

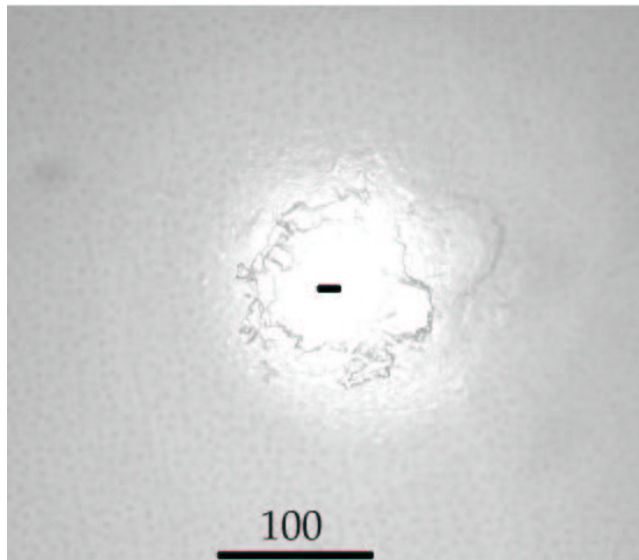


Figure 3. Small-scale features on top of a parabolic polypropylene die. The bars are 100 μm and 15 μm .

The parabolic dies are injection-molded polypropylene. This material was chosen because lithium does not stick to purely hydrocarbon-based plastics, and of these polypropylene is the hardest. With suitable lubricants such as (anhydrous) hexane or nonane it is possible to emboss lithium with dies made from steel or other conventional, strong, materials, but polypropylene was chosen to avoid contaminating the 152 surfaces of the 76-lenslet CRL with lubricant.

It was not possible to verify that the lithium lenslets have the desired parabolic profile, or to assess the quality of the surface quantitatively. Figure 3 is the top of a typical parabolic die seen under an optical microscope. It shows a circular structure, a halo, with as smallest length scale its transverse dimension on the order of a few microns. Embossing should transfer these features to the lithium, but we have not been able to correlate structure of the die with that of the lithium.

Lithium's rapid corrosion under normal circumstances makes it difficult to keep lithium's surface quality. In dry air with less than $\simeq 1000$ ppm humidity lithium is protected by an oxide layer. Earlier lenses used lithium with whatever oxide layer was present after the material was extruded in dry air at the supplier, but in an attempt to minimize surface oxidation the lenses here were made with lithium extruded in dry helium. The finished lithium CRL is mounted in its hermetic enclosure inside the glove box.

The measurement setup for the CRL is straightforward.¹⁸ Briefly, monochromatic x-rays from the Advanced Photon Source's (APS's) beam line 7-ID pass through various beryllium and kapton windows, and enter the lens through a rectangular aperture 25 mm in front. A YAG:Ce scintillating screen converts the x-rays into visible light, which is gathered by a CCD at $5\times$ magnification. This setup is ideal to quickly focus the beam, and adequate to evaluate the lens's quality from the shape of the x-ray source's image. The signal from the CCD is proportional to the x-ray intensity up to 75 % of full scale (3000 counts out of 4096), but sometimes the intensity in the focal spot is outside the linear range. In part for this reason the x-ray intensity gain quoted in this paper is an underestimate. The actual gain must be confirmed with other techniques in future measurements.

At 10 keV lithium's index of refraction decrement $\delta \simeq 0.95 \times 10^{-6}$, hence a parabolic lens with $N = 76$ lenslets of radius $R_0 = 0.263$ mm has its focus at $f = R_0/(2N\delta) \simeq 1.82$ m. The lens formula $1/f = (1/d_i + 1/d_s)$ puts the image from a source at $d_s = 49.4$ m in front of the lens at $d_i = 1.89$ m behind the lens. However, the smallest visible spot is at 1.52 m (measured from the exit plane of the 100 mm long lens), 300 mm closer than expected. The reason for the discrepancy is not clear. However, $R_0 = 0.263 \mu\text{m}$ is the radius of curvature specified for the die, not the actual radius of curvature of the lithium which could not be measured. The radius of curvature

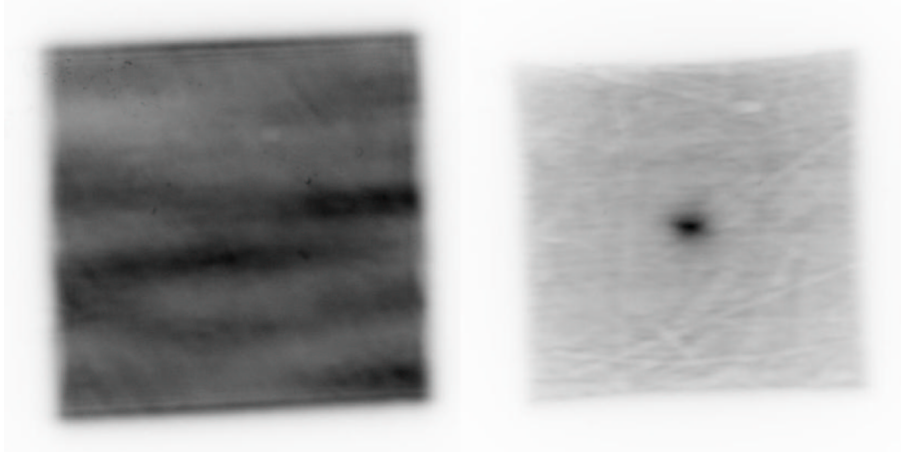


Figure 4. Original x-ray beam without (left) and with the lens and an x-ray filter 1.52 m downstream (right).

could have become slightly smaller R_0 than intended because the polypropylene die may have distorted during molding: it is not ideally stiff. The lens's $L \simeq 0.1$ m length gives the focal length a $L/6 \simeq 16$ mm correction that makes no difference.

Figure 4 compares the x-rays before and after the lens. The left part of the figure is the beam without the lens, as limited by a $500 \mu\text{m}$ square aperture $\simeq 25$ mm in front of the lens position. At the diagnostics 1.52 m downstream this beam is magnified by the geometry to a $515 \mu\text{m}$ square. The x-ray source is an order of magnitude wider (FWHM $478 \mu\text{m}$) than it is high (FWHM $33 \mu\text{m}$), the coherence is larger in the vertical than in the horizontal, and Fresnel fringes are visible only along the top and bottom edges. Thanks to ongoing improvements of the x-ray beam line, the beam's horizontal striations are much smaller than during previous measurements:¹³ they should be smaller still in future work.

The right part of Figure 4 is the x-ray beam 1.52 m behind the lens, filtered by an aluminum attenuator to bring the beam's intensity into a convenient range and makes the harmonics conveniently visible. For the 10 keV fundamental x-rays the attenuation by 18 layers of $38.1 \mu\text{m}$ aluminum foil is almost 250-fold, but the 30 keV harmonics are barely ($1.2\times$) affected. When the harmonics are visible it is easy to orient the refractive lens, because the harmonics show where the x-ray beam is. For a cylindrically symmetric lens the focus is on the lens's optical axis, so that a focal spot in the center of the harmonic beam implies that the optical axis is aligned with the beam.

X-ray refraction is chromatic, since the index of refraction decrement δ decreases $\propto 1/(h\nu)^2$ with photon energy $h\nu$. The dominant 30 keV harmonic deflects $1/9^{\text{th}}$ less than the fundamental, hence a lens that focuses 10 keV x-rays makes a 30 keV x-ray beam smaller by a factor $1 - (1/3)^2 = 8/9$. In Figure 4 the background square has the expected width and height, but along the diagonals it is slightly larger. The square's distortion is consistent with the lens's figure errors at the edge of the aperture discussed later on.

For ideal focusing the 10 keV fundamental x-rays should form a demagnified image of the source, with a demagnification factor $M = d_s/d_i \simeq 32.5$. The source's FWHM is $478 \mu\text{m}$ horizontal and $33 \mu\text{m}$ vertical, hence the ideal image is a $\simeq 15 \mu\text{m}$ long needle of $\simeq 1 \mu\text{m}$ height. The resolution of the diagnostics¹⁸ is $\simeq 5 \mu\text{m}$, and the expected image is $15.5 \mu\text{m}$ wide by $5 \mu\text{m}$ high.

Figure 5 shows the horizontal (solid) and vertical cross section (dashed) through the bright spot in Figure 4. Horizontally the FWHM is $36 \mu\text{m}$, $20 \mu\text{m}$ larger than expected. The vertical FWHM is $26 \mu\text{m}$, also $20 \mu\text{m}$ too large. These widths are consistent with an image widened by isotropic small angle scattering, with an angle $\simeq 13 \mu\text{radians}$.

The lithium lens is a very useful collimator thanks to its 50-fold intensity gain G . The value for G is calculated from the images like those in Figure 4, taking into account the absorption in the aluminum filter for 10 keV

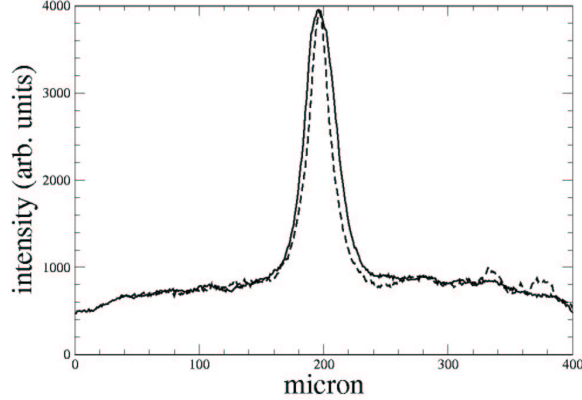


Figure 5. Cross sections in x (solid) and y (dashed) through the focused beam on the right side of Figure 4.

x-rays (0.0041 for Figure 4) and the CCD's integration time (10 ms for the initial beam to the left, 75 ms for the focused beam to the right in Figure 4). In these images the CCD is overexposed, hence the image seems bigger than it really is, and the gain is underestimated. Other diagnostic types that measure widths and x-ray fluences independently could not be installed during this run.

While a gain $G \simeq 50$ is appreciable, it is an order of magnitude lower than what is theoretically possible ($G \simeq TM^2 \simeq 500$, with transmission $T \simeq 0.5$), and the difference in gains points to problems with lens fabrication.

One fabrication problem is insufficient accuracy in locating the individual lenslets along a common axis. The CRL is made by stacking N individual lenslets with thickness $z_i = [(x - x_i)^2 + (y - y_i)^2]/(2R) + z_{0i}$, each with the same parabolic radius of curvature R but centered at random positions (x_i, y_i) and with individual dead layers z_{0i} . When the center of the coordinate system is chosen such that $\sum x_i = 0$ and $\sum y_i = 0$, the lens stack is¹⁹ $z(x, y) = \sum z_i(x, y) = (x^2 + y^2)/2R_N + z_0$ thick, i.e., a parabola with radius $R_N = R/N$, and dead layer $z_0 = \sum z_{0i} + (\sum x_i^2)/(2R/N)$. The dead layer is thicker than the minimum $\sum z_{0i}$ by a term that is quadratic in the x_i 's and y_i 's, hence negligibly small when the positioning errors are much smaller than the other lens dimensions.

Lithium is so transparent to x-rays that the lens's 1 mm physical aperture is comparable to the CRL's absorption aperture. Misalignment now matters, because x-rays at the edge of the aperture pass through the flat part of some lenslets, outside the parabolic profile that applies only within $r = \sqrt{x^2 + y^2} = 0.5$ mm of each lenslet's individual optical axis. Such x-rays do not deflect far enough to converge at the focus, and this becomes wider.

Macroscopic figure errors like these are most clearly seen when the lens is probed locally, with a small x-ray beam. Figure 6 demonstrates the effect. The top of the figure indicates where the nominally 20 μm square x-ray beam goes through the lens, along a horizontal cross section through the optical axis. The section of the circle (solid) gives the desired 1000 μm aperture for the lens, while the dashed circle-cuts suggest apertures of individual lenslets that are randomly shifted by $\simeq 50$ μm .

The lower part of the figure shows the small beam's image for each position indicated at the top, every 100 μm across the lens, but displaced vertically so that the images are visible separately. The x-ray beam is again filtered with aluminum. The harmonic radiation deflects $1/9^{\text{th}}$ as much as the fundamental, hence the undeflected beam is $1/8^{\text{th}}$ as far from the harmonic image as the fundamental image, and on the opposite side.

The three beams on each side of the aperture (marked $\pm 7 \pm 1$) go through the flat part outside the lens, see Figure 2. Neither the fundamental x-rays nor the harmonic x-rays deflect, hence the image is a single bright spot. In the other images the bright spot comes from the fundamental x-rays, while the weak spot is from the

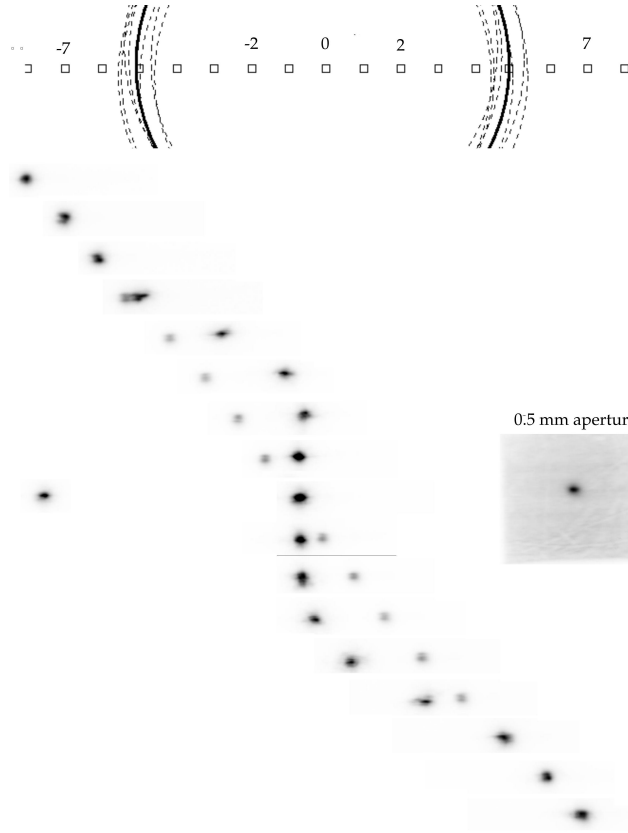


Figure 6. Images from a nominally $20\ \mu\text{m}$ square x-ray beam, focused by the lens's local profile spaced at $100\ \mu\text{m}$ intervals along a lens diameter.

harmonics and indicates the x-ray beam. They are on a straight line that is consistent with the incremental $100\ \mu\text{m}$ shift of the lens with respect to the beam.

Close to the edge of the aperture the lens is thicker, and the x-rays away from the center attenuate more than the x-rays going through the center of the lens. Since all the images are taken with the same sensitivity of the diagnostics, those closest to the center are overexposed and seem larger than they really are. The image on the left is the central spot of the $20\ \mu\text{m}$ wide beam at reduced exposure ($0.3\times$ of the other images). The spot is now about the same size as the other marginally saturated images. To the right is Figure 4 on the same spatial scale, the $500\ \mu\text{m}$ square beam passing through the lens (taken at $25\times$ reduced sensitivity).

The x-ray images directly show the quality of the lens close to the physical aperture, by the split between the fundamental and the harmonic x-rays. The 10 middle images are clearly within the lens aperture, but $\pm 100\ \mu\text{m}$ to the side the x-rays hit the aperture's edge. The actual lens profile is then $1000\ \mu\text{m}$ to $1200\ \mu\text{m}$ wide, nominally $100\ \mu\text{m}$ larger than the physical $1000\ \mu\text{m}$ aperture of each individual lenslet.

For an ideal lens the focal spots of the fundamental x-rays from any position across the lens must line up, on the optical axis. In Figure 6 the 5 spots in the figure's center (between ± 2) line up properly, perhaps with a shift that is much smaller than the x-ray spot itself. But, closer to the $1000\ \mu\text{m}$ aperture the lens deflects the x-rays less than it should.

Figure 6 suggests a random misalignment of the $N = 76$ individual lenslets, by about $\simeq 100\ \mu\text{m}$. X-rays passing through the lens within $\simeq 100\ \mu\text{m}$ or $200\ \mu\text{m}$ inside the aperture go through the parabolic part of some lenslets, and through the flat lithium of other lenslets. The net effect is a deflection that decreases as the x-rays



Figure 7. A nominally $20\ \mu\text{m}$ square x-ray beam focused by the lens $200\ \mu\text{m}$ above (left image) and below the optical axis (right image).

get closer to the edge. A Gaussian distribution of misalignments should give the deflected spots an error function distribution, as is seen in the inverted 'S'-shape of the x-ray spots.

Errors of $\simeq 100\ \mu\text{m}$ are consistent with the stamping accuracy of the lenslet holders, the quality of the machining in the alignment fixture used to emboss the lenslets, and the positioning of the dies in this fixture. It should be straightforward to improve lenslet alignment with a mold table and a procedure to stack the lenslets without counting on their azimuthal symmetry.

In principle the random shifts of the lenslet apertures could also come from errors in fabricating the individual lenslets. Numerical modeling²⁰ of lithium's flow during the embossing process, and common sense in guessing the flow patterns in looking at Figure 2, shows that lithium first surrounds the parabola's tops, and only later flows toward the lenslet's outer edge. Insufficient pressure on the die, or insufficient time for the lithium to flow, could then lead to less lithium in random places at a lenslet's edge. While the lenslets that make up the lens are all visually acceptable, looking at the lenslets through a loupe at $5\times$ magnification may not be good enough to see imperfect filling.

Macroscopic errors in the lens figure reduce the gain by widening the focal spot, but they do not affect the

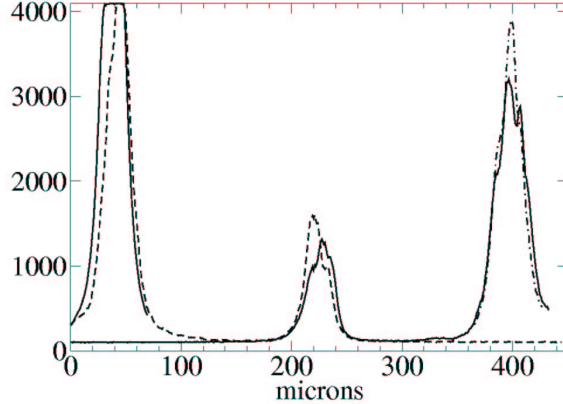


Figure 8. Cross sections through the image of the 10 keV x-rays and the original beam in the harmonics seen in Figure 7.

image of a small beam. Figure 7 shows two samples of the bright image in the fundamental x-rays, together with the background from the beam's higher harmonics, for a nominally $20\ \mu\text{m}$ square beam as in Figure 6. This time the left image is for a beam that goes through the lens $200\ \mu\text{m}$ below the optical axis, the right image for the beam at $200\ \mu\text{m}$ above the optical axis.

For these two beams the lens is macroscopically parabolic enough that the fundamental x-rays deflect the same distance, in opposite directions. But, the images differ and the lens surface in the two spots differs too. The image on the right side is marginally wider than expected, perhaps in part due to overexposure of the CCD, but the image on the left is twice wider than it should be. In addition, the left image has vertical structure than the right image lacks. Related differences are visible in the harmonics. Apparently, the lens is may be sufficiently parabolic over the beam's $20\ \mu\text{m}$ square footprint for the right image, but not for that on the left.

Figure 8 compares the cross sections of the original beam with that of the images seen in Figure 7. The bottom image, in this cross section detail on the left, is quite narrow and slightly overexposed. The solid line with $\text{FWHM} \simeq 31\ \mu\text{m}$ is a horizontal cross section through the image's center, the dashed line with $\text{FWHM} \simeq 22\ \mu\text{m}$ a vertical cross section that also goes through the harmonic beam.

The nominally $20\ \mu\text{m}$ square harmonic beam in the center is blurred, both by the $\simeq 5\ \mu\text{m}$ resolution of the diagnostic and by diffraction around the limiting slits. Although refraction affects the harmonic x-rays $1/9^{\text{th}}$ as much as the fundamental, the harmonic beams that passed through the different parts of the lens are visibly different. They are overlaid for comparison: the harmonic beams are displaced from the optical axis by $1/9$ of $200\ \mu\text{m}$ or approximately $20\ \mu\text{m}$. Therefore the focal spots in this figure seem to be $360\ \mu\text{m}$ apart, not $400\ \mu\text{m}$.

To the right in Figure 8 is the cross section through the top image in Figure 7. The solid line is a vertical cut that includes the harmonic beam, the dash-dotted line a second vertical cut through the image's maximum. Their FWHMs are $34\ \mu\text{m}$ and $27\ \mu\text{m}$. The dashed line on the left is a vertical cut through the lower image and the corresponding harmonic beam. It is more intense than the upper image, and overexposed since they are on the same scale. Its FWHM is $22\ \mu\text{m}$, consistent with the $\simeq 20\ \mu\text{m}$ widening by small-angle scattering already inferred earlier. The solid line to the left is a horizontal cross section through the lower image. Its FWHM is $29\ \mu\text{m}$, about twice as large as the ideal image and also consistent with a $\simeq 20\ \mu\text{m}$ scatter.

The bottom spot in Figure 7 shows that small x-ray scattering is a local property of the lens, but it does not determine its cause: scatter can come from roughness of the lens surface, or from non-uniformities of the lithium itself. Inspection of the individual lenslets should give further insight, but to date it has not been possible to do such measurements properly (e.g., inside the glove box, or with standard equipment that allows an inert atmosphere). Surface oxydation of the lithium is always a suspect, but comparable small-angle scattering was

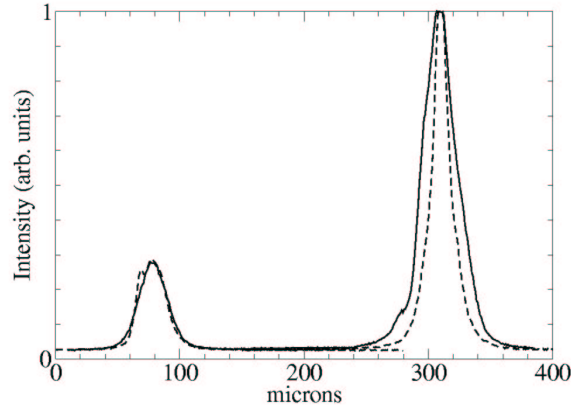


Figure 9. Cross section of harmonic beam and fundamental x-ray image from a lens region $300 \mu\text{m}$ outside the optical axis.

observed in an earlier version¹³ of the lens. The lenslets for earlier tests were made from lithium strips extruded in dry air, while in an attempt to minimize oxide layers the present lens uses strips extruded inside the glove box. Unfortunately, this improvement in lens fabrication does not suppress small-angle scattering.

The polypropylene die's roughness is less than 25 nm . Since embossing should faithfully reproduce surfaces (consistent with reflection of visible light from both the lithium and the die), the surface quality of the lenslet is assumed to be 25 nm too. Specular reflection of visible light demonstrates that the surface quality of a CRL is sufficient for x-ray refraction. Electromagnetic radiation with wave length λ reflecting from a given surface with roughness Δ scatters over a characteristic angle λ/Δ , while radiation entering from vacuum through this same surface into a material with index of refraction n scatters over $\lambda(n-1)/\Delta$. For visible radiation $\lambda \simeq 1 \mu\text{m}$ is 10^4 larger than for 10 keV x-rays, but their $(n-1) = \delta \simeq 10^{-6}$. A CRL with $N \simeq 76$ identical but randomly oriented lenslets scatters $\sqrt{2N} \simeq 13$ times more than a single surface, but still over an angle that is one order of magnitude less than for visible light reflecting from one such surface. While it is emotionally satisfying to see a mirror-like lithium surface, a quantitative measurement of how well the lithium surface reflects light remains to be done.

Even though the lens does not bring all the x-rays to the optical axis over its entire aperture, as in Figure 6, some parts of the lens image quite well. As an example, Figure 9 is the cross section for the $20 \mu\text{m}$ square beam at position -3 in Figure 6, with the beam going through the lens $300 \mu\text{m}$ to the left of the optical axis. The solid line is a horizontal cut through both maxima, the dashed lines are cross sections through the same point along the vertical. The harmonic beam is $26 \mu\text{m}$ wide. This is slightly larger than $18 \mu\text{m}$, the size in geometrical optics expected from the geometry, the nominal $20 \mu\text{m}$ slit setting, and the $1/9^{\text{th}}$ reduction in size due to the lens. Non-ideal contributions that could widen the image include diffraction at the edge of the aperturing slit $\simeq 1.75 \text{ m}$ upstream of the diagnostics, some uncertainty about its actual aperture, and imperfect tuning of the diagnostics (optical focusing, overexposure of the CCD) that may lower its resolution from a nominal $4 \mu\text{m}$ to something larger. Still, one good image is encouraging, since it suggests that nothing seems to be fundamentally wrong with lithium as an x-ray optics material.

Lithium is not an amorphous material like glass, and in principle lithium metal could suffer from imperfections that may affect the phase of the x-rays in unintended ways. Experts on lithium metallurgy^{16,17} assure us that crystals in pure metallic lithium at room temperature are relatively large, 1 mm or so, and just about the size as an individual lenslet. In this case each lenslet can be a single crystal, and the lens material should be homogeneous. While the lithium used in the CRL is the highest available commercial quality, it has not been purified further. Hence it seems possible that the remaining impurities conspire with the deformations needed

to emboss parabolas to leave the lithium with smaller crystals that have not annealed away, dislocations in the individual crystals, and similar features that metallurgists worry about.

Despite these various shortcomings of the lithium lenses that as yet hinder their application to imaging, the lithium CRLs could be ideal for applications where their $\approx 50\%$ throughput, fifty-fold intensity gain, price, and ease of use are the principal requirements.

ACKNOWLEDGMENTS

We thank Mr. N. S. Liu (MoldBridge Associates) for making the parabolic molds in polypropylene, and Prof. T. Turng and Andreas Winardi (University of Wisconsin's NSF Center for Applied Polymer and Composites Engineering) for their contributions to lithium's manufacturing technology. NRP was supported by MDA through SBIR contract N00178-02-C-3119, which was monitored by the Naval Surface Warfare Center, Dahlgren Division.

Operation of the MHATT-CAT Sector 7 beamlines at the Advanced Photon Source is supported by DOE Grant No. DE-FG02-03ER46023. Use of the Advanced Photon Source is supported by the U.S. Department of Energy, Basic Energy Sciences, Office of Energy Research, under Contract No. W-31-109-ENG-38.

REFERENCES

1. S. Suehiro, H. Miyaji, and H. Hayashi *Nature* **352**, p. 385, 1991.
2. A. Snigirev, V. Kohn, A. Snigireva, and B. Lengeler, "A compound refractive lens for focusing high-energy x-rays," *Nature* **384**, p. 49, 1996.
3. V. G. Kohn, "An exact theory of imaging with a parabolic continuously refractive x-ray lens," *J. Exp. Theor. Phys.* **97**, p. 224, 2003.
4. B. Lengeler, C. Schroer, J. Tuemmler, B. Benner, M. Richwin, A. Snigirev, I. Snigireva, and M. Drakopoulos, "Imaging by parabolic refractive lenses in the hard x-ray range," *J. Synchrotron Rad.* **6**, p. 1153, 1999.
5. C. G. Schroer, J. Meyer, M. Kuhlmann, B. Benner, T. F. Guenzler, B. Lengeler, C. Rau, T. Weitkamp, A. Snigirev, and I. Snigireva, "Nanotomography based on hard x-ray microscopy with refractive lenses," *Appl. Phys. Lett.* **81**, p. 1527, 2002.
6. C. G. Schroer, M. Kuhlmann, U. T. Hunger, T. F. Günzler, O. Kurapova, S. Feste, F. Frehse, B. Lengeler, M. Drakopoulos, A. Somogyi, A. S. Simionovici, A. Snigirev, I. Snigireva, C. Schug, and W. H. Schröder, "Nanofocusing parabolic refractive x-ray lenses," *Appl. Phys. Lett.* **82**(9), pp. 1485–1487, 2003.
7. B. Lengeler, C. G. Schroer, M. Kuhlmann, B. Benner, T. F. Günzler, O. Kurapova, A. Somogyi, A. Snigirev, and I. Snigireva, "Beryllium parabolic refractive x-ray lenses," in *Synchrotron Radiation Instrumentation*, T. Warwick, J. Arthur, H. A. Padmore, and J. Stöhr, eds., *AIP Conference Proceedings*(705), pp. 748–751, 2004.
8. B. Cederstrom, R. Cahn, M. Danielsson, M. Lundqvist, and D. Nygren, "Focusing x-rays with lps," *Nature* **404**, p. 951, 2000.
9. B. Cederstrom, M. Lundqvist, and M. Ribbing, "Multi-prism x-ray lens," *Appl. Phys. Lett.* **81**, p. 1399, 2002.
10. B. X. Yang *Nucl. Instrum. Meth.* **A328**, p. 578, 1993.
11. E. M. Dufresne, D. A. Arms, S. B. Dierker, R. Clarke, N. R. Pereira, and D. Foster, "Lithium metal for x-ray refractive optics," *Appl. Phys. Lett.* **79**, p. 4085, 2001.
12. D. A. Arms, E. M. Dufresne, S. B. Dierker, R. Clarke, N. R. Pereira, and D. Foster, "Refractive optics using lithium metal," *Rev. Sci. Instrum.* **73**, p. 1492, 2002.
13. N. R. Pereira, E. M. Dufresne, D. A. Arms, and R. Clarke, "Parabolic lithium refractive optics for x-rays," *Rev. Sci. Instrum.* **75**, p. 37, 2004.
14. J. T. Cremer, H. R. Beguiristain, M. A. Piestrup, and C. K. Gary, "Large aperture compound refractive lenses made of lithium," *Rev. Sci. Instrum.* **74**, p. 2262, 2003.
15. S. Tariq, K. Ammigam, P. Huhner, R. Schultz, P. Liu, and J. Chang, "Li material testing - fermilab antiproton source lithium collection lens," *Proc. 2003 Particle Accelerator Conference* **62**, p. 1452, 2003.
16. M. Krystian and W. Pichl, "In situ optical microscopy of the martensitic phase transition of lithium," *Phys. Rev. B* **62**, p. 13956, 2000.

17. M. Krystian and W. Pichl, "Metallography of alkali metal single crystals," *Materials Characterization* **46**, p. 1, 2001.
18. E. M. Dufresne, N. R. Pereira, and D. Arms, "Two-dimensional multiprism x-ray collimator from lithium," *Proc. 2003 SRI Conference and AIP Conference Proceedings* **705**, p. 780, 2004.
19. R. H. Pantell, J. Feinstein, H. R. Beguiristain, M. A. Piestrup, C. K. Gary, and J. T. Cremer, "The effect of unit lens alignment and surface roughness on x-ray compound lens performance," *Rev. Sci. Instrum.* **72**, p. 48, 2001.
20. A. Winardi and T. Turng, "Deform calculations on extruding lithium metal," *Report to Ecopulse (unpublished)* , 2003.